Local and Closed-Loop Calibration of an Industrial Serial Robot using a New Low-Cost 3D Measuring Device*

Martin Gaudreault, Ahmed Joubair, and Ilian A. Bonev

***Abstract*—We propose an automated, closed-loop, and local calibration method for serial robots that uses a new, low-cost, 3D measuring device. The device consists of three Mitutoyo digital indicators, arranged in an orthogonal manner, and a mastering fixture based on kinematic coupling. The indicators communicate, via wireless connection, with a PC that controls the movements of the robot. To measure absolute Cartesian coordinates, the device is positioned incrementally over each of several 0.5-inch precision balls until all indicators are at zero, at which time the robot joint encoders are read. The balls are fixed with respect to the robot's base. The precise relative positions of the centers of these balls must be known in advance. In this study, the measuring device is mounted on the flange of an ABB IRB 120 robot. Only three precision balls are used, spaced 300 mm apart, and the distances between these balls are measured with a Renishaw telescoping ballbar. The absolute accuracy of the robot was enhanced by minimizing its position errors, using the least squares method. The feasibility of the calibration approach was demonstrated through a simulation study. Finally, an experimental validation showed that our calibration method caused the maximum position error of the robot, inside a sphere of 400 mm in diameter, to be reduced to 0.491 mm.**

I. Introduction

Industrial robot programming methods have evolved greatly over recent decades. In the past, each pose had to be taught to the robot manually. The resulting poses were highly precise because they relied on the robot's excellent repeatability; but manual teaching tasks are time-consuming and difficult to adapt for complex operations. Today, almost every robot manufacturer provides customized 3D simulation software, allowing industrial robots to be programmed entirely offline. Simulations have greatly benefitted the manufacturing industry, since they reduce production down-time and allow complex operations to be accomplished.

However, the improvements in simulation software have not solved all the problems of robotic programming, particularly for applications requiring high levels of accuracy. One cannot depend solely on offline programming, because when the robot's pose is calculated offline, it relies on the accuracy of the robot, which is worse than the robot's repeatability by a large-scale factor.

To remedy this problem, manufacturers typically perform a calibration to decrease the gap that exists between the repeatability and the accuracy of the robot. The basic steps of robot calibration have been clearly defined [1, 2], and are the same for any robot – modeling, measurement, identification and implementation.

*Corresponding author: ilian.bonev@etsmtl.ca. This work was financially supported by Canada Research Chairs, Canada Foundation for Innovation, the Fonds de recherche du Québec – Nature et technologies, and ÉTS.

First, a mathematical model of the robot must be defined. There are many different models used for calibration of serial robots. While most are based on the Denavit-Hartenberg parameters [3, 4], many researchers have also defined their own models [5-7].

The second step is to use a measuring device to gather measurements in the robot's workspace. Based on our experience, we believe the ideal device should measure the position of the tool center point (TCP) within the whole workspace of the robot. Such a device must meet several requirements, if it is to be commercially viable: it must be highly accurate (0.1 mm or better), portable, and inexpensive, and the measurement process must be relatively fast (less than an hour), easily implemented, and fully automated.

We classify the actual measurement methods into two categories: in-contact, and non-contact. The in-contact measuring devices must be constrained at specific physical poses to collect measurements, whereas the non-contact measuring devices do not need to be constrained. In-contact measuring devices are sometimes preferred, because of their lower price and higher accuracy; but non-contact measuring devices have the advantage of being able to measure positions within the robot's whole workspace. The in-contact measuring devices that are typically used in robot calibration are Coordinate Measuring Machines (CMM) [8], articulated measurement arms [9], touch probes [10, 11] and telescoping ballbars [12, 13]. The non-contact measuring devices that are used most often in robot calibration are laser trackers [14], optical CMMs [14] and stereo-vision systems [15].

The third step of robot calibration is the identification process. The measurements collected by the measuring device are used to identify the robot's parameters, typically through applying the least squares optimization techniques [16, 17]. Finally, the last step is to compensate the end-effector errors by calculating so-called *fake targets*.

In this work, we present a new in-contact and closed-loop measuring device, that we have named the *TriCal*. It is used to gather accurate 3D position measurements for calibration of industrial robots. The *TriCal* includes three orthogonally-arranged Mitutoyo digital indicators that are used to measure the coordinates of a precision ball with respect to the device, by probing. The *TriCal* device is thus highly accurate, as each indicator has a resolution of 0.001 mm.

If there is one drawback to the *TriCal*, it is that, in practice, measurements can only be made within a limited target workspace (e.g., using only three precision balls), and not the whole robot workspace (e.g., using twenty balls). However, since many tasks are suited to this constraint (*i.e.*, they are performed within a small portion of the robot's workspace), we believe the *TriCal* will be broadly applicable.

While devices similar to ours have existed for decades [18], to the best of our knowledge, none include a calibrator plate, meaning that the precise position and orientation of each indicator stem must be known. Since our device does not require this information, it is far less expensive (about US$5,000). Furthermore, the measurement process is easy to automate, and it is does not take much time to complete (about 20 seconds per measurement).

Most importantly, however, *TriCal* is used to position the robot's TCP to known reference points (precision balls) as in [19, 20]. However, in contrast to [19, 20], our procedure does not require a continuous physical constraint of the TCP at the point of measurement. Thus, force control is not required to move the robot between different configurations.

This paper begins by introducing the robot model. Then, the experimental setup is described and the new measuring device and the automated measuring process are detailed. Next, we present a random configuration generation algorithm, and assess the effector of the measuring noise. Finally, we present a real calibration with the new measuring device, and validate the results with a laser tracker.

II. Robot Model

The following section presents the nominal kinematic model of the robot, and details the kinematic and non-kinematic errors that were selected for identification.

A. Kinematic Model

The calibration process is applied to the ABB IRB 120 (Fig. 1), a six-degrees-of-freedom (6-DOF) small serial industrial robot. This robot is comprised of six revolute joints, and its kinematic model is developed according to the Modified Denavit-Hartenberg (MDH) approach, as presented in [21]. This model involves nine reference frames: the world frame {*W*}, the base frame {0}, the tool frame {*tool*}, and the six link frames {1}, {2}, …, {6}.

The origin of the frame {*W*} is located at the center of precision ball 1. As shown in Fig. 1, its *x* axis points toward the center of ball 2, and its *y* axis is in the plane formed by the centers of balls 1, 2 and 3. These are the balls that will be probed with our device. The *x*, *y* and *z* axes of {tool} are defined as aligning with the axes of the stems of the three digital indicators.

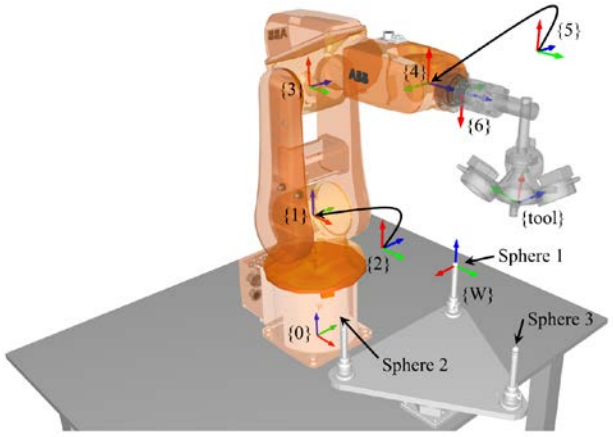

Figure 1. Reference frames of the IRB 120 robot.

Given the vector of the joint variables,

$$\mathbf{q} = \left[\theta_1, \theta_2, ..., \theta_6\right]^T, \quad (1)$$

the end-effector's pose {*tool*} with respect to (w.r.t.) {*W*} is

$$\mathbf{T}_{tool}^{W}(\mathbf{q}) = \mathbf{T}_{0}^{W}\mathbf{T}_{6}^{0}(\mathbf{q})\mathbf{T}_{tool}^{6}, \quad (2)$$

where $\mathbf{T}_j^i$ is the homogeneous matrix representing the pose of frame {*i*} w.r.t. frame {*j*}.

Thus, matrix $\mathbf{T}_6^0$ is calculated as follows:

$$\mathbf{T}_{6}^{0}(\mathbf{q}) = \mathbf{T}_{1}^{0}(q_1)\mathbf{T}_{2}^{1}(q_2)\mathbf{T}_{3}^{2}(q_3)\mathbf{T}_{4}^{3}(q_4)\mathbf{T}_{5}^{4}(q_5)\mathbf{T}_{6}^{5}(q_6). \quad (3)$$

For $i = 1, 2, \ldots, 6$, the MDH parameters are used to obtain the homogenous matrix linking each successive pair of frames,

$$\mathbf{T}_{i}^{i-1} = \mathbf{R}_{\mathrm{x}}\left(\alpha_{i-1}\right)\mathbf{Trans}\left(a_{i-1},0,0\right)\mathbf{R}_{\mathrm{z}}\left(\theta_i\right)\mathbf{Trans}\left(0,0,d_i\right) \quad (4)$$

$$\mathbf{T}_{i}^{i-1} = \begin{bmatrix} \mathrm{c}\theta_i & -\mathrm{s}\theta_i & 0 & a_{i-1} \\ \mathrm{s}\theta_i \mathrm{c}\alpha_{i-1} & \mathrm{c}\theta_i \mathrm{c}\alpha_{i-1} & -\mathrm{s}\alpha_{i-1} & -d_i \mathrm{s}\alpha_{i-1} \\ \mathrm{s}\theta_i \mathrm{s}\alpha_{i-1} & \mathrm{c}\theta_i \mathrm{s}\alpha_{i-1} & \mathrm{c}\alpha_{i-1} & d_i \mathrm{c}\alpha_{i-1} \\ 0 & 0 & 0 & 1 \end{bmatrix} \quad (5)$$

where α_{i-1}, a_{i-1}, θ_i and d_i are the MDH parameters and $\mathrm{s}\theta_i = \sin(\theta_i)$, $\mathrm{c}\theta_i = \cos(\theta_i)$, etc. Table I gives the nominal MDH values, and Table II gives the nominal parameters linking {0} to {*W*} and {*tool*} to {6}.

TABLE I. Nominal values of the MDH parameters of the IRB 120 robot

i	α_{i-1} (°)	a_{i-1} (mm)	d_i (mm)	θ_i (°)
1	0	0	290	θ_1
2	− 90	0	0	$\theta_2 - 90$
3	0	270	0	θ_3
4	− 90	70	302	θ_4
5	90	0	0	θ_5
6	− 90	0	72	$\theta_6 + 180$

TABLE II. Nominal pose parameters of {0} w.r.t. {W} and {tool} w.r.t. {6}

Parameters	Nominal Values
x_0 (mm)	153.507
y_0 (mm)	−256.442
z_0 (mm)	−228.116
α_0 (°)	90.487
β_0 (°)	−1.054
φ_0 (°)	−0.165
x_{tool} (mm)	149.679
y_{tool} (mm)	1.859
z_{tool} (mm)	120.806
α_{tool} (°)	0.000
β_{tool} (°)	90.000
φ_{tool} (°)	0.000

*α, β and φ are the Euler angles, according to the ZY'X'' convention.

B. Assessment of kinematic and non-kinematic errors

Our calibration takes 26 kinematic errors and 5 non-kinematic errors into account, as shown in Tables III and IV. No kinematic errors are considered for link 1, since those parameters are interdependent with the parameters modeling the base w.r.t. the world frame. Because the position and orientation of the base must be identified, they cannot be included in the model. Also, axes 2 and 3 are parallel, so to avoid redundancy, only one of either δd_2 or δd_3 should be included in the calibration model (we chose to remove δd_2). Errors δd_6 and $\delta\theta_6$ were not included in the model because they are interdependent with the position parameters of the tool that need to be identified. The tool's orientation is not included because our device only gives us information about its position.

To model the elasticity in each gearbox, five non-kinematic errors were considered for joints 2–6. The elasticity in each gearbox is modeled as a linear torsional spring, as in [18]. Because the joint 1 axis is parallel to the direction of gravity, no torque is applied when the robot is stationary. Thus, no non-kinematic error parameter is associated with this joint.

III. Experimental Setup

The experimental setup consists of three main components, as shown in Fig. 2: the ABB IRB 120 robot, a triangular platform, and the new measuring device.

TABLE III. MDH parameters with kinematic and non-kinematic errors

i	α_{i-1} (°)	a_{i-1} (mm)	d_i (mm)	θ_i (°)
1	0	0	290	θ_1
2	$-90+\delta\alpha_1$	δa_1	0	$\theta_2-90+\delta\theta_2+c_2\tau_2$
3	$\delta\alpha_2$	$270+\delta a_2$	δd_3	$\theta_3+\delta\theta_3+c_3\tau_3$
4	$-90+\delta\alpha_3$	$70+\delta a_3$	$302+\delta d_4$	$\theta_4+\delta\theta_4+c_4\tau_4$
5	$90+\delta\alpha_4$	δa_4	δd_5	$\theta_5+\delta\theta_5+c_5\tau_5$
6	$-90+\delta\alpha_5$	δa_5	72	$\theta_6+180+c_6\tau_6$

TABLE IV. Parameters considered for the base and the tool, with their nominal values and error parameters

Parameters	Value
x_0 (mm)	$153.507+\delta x_0$
y_0 (mm)	$-256.442+\delta y_0$
z_0 (mm)	$-228.116+\delta z_0$
α_0 (°)	$90.487+\delta\alpha_0$
β_0 (°)	$-1.054+\delta\beta_0$
φ_0 (°)	$-0.165+\delta\varphi_0$
x_{tool} (mm)	$149.679+\delta x_{tool}$
y_{tool} (mm)	$1.859+\delta y_{tool}$
z_{tool} (mm)	$120.806+\delta z_{tool}$
α_{tool} (°)	0.000
β_{tool} (°)	90.000
φ_{tool} (°)	0.000

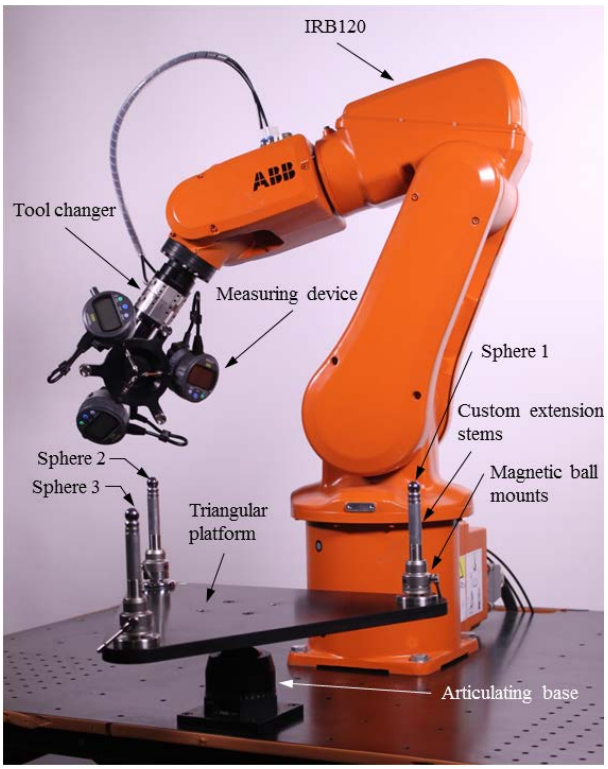

Figure 2. *TriCal*'s measuring device, installed on the IRB 120 robot, with the triangular platform installed on the table.

A. Triangular platform

The robot is fixed to steel table, and so is a triangular platform, via an articulating base that allows us to change the platform's orientation. In our experiment, the platform is installed parallel to the robot's base. Each of the three 0.5-inch precision balls is installed on a magnetic mount. The mounts are placed at the three corners of the triangular platform. We chose to space them 300 mm apart, for two reasons: we wanted to be able to measure this distance accurately with our QC20-W Renishaw telescoping ballbar, and we wanted to enable collision-free measurements for any end-effector pose on the three precision balls (spheres). The height of the spheres w.r.t. the platform was selected so that our measuring device could rotate as freely as possible around the spheres, without colliding with the platform.

B. TriCal – A new in-contact measuring device

To collect accurate measurements, we developed a new in-contact measuring device, which we have named the *TriCal* (https://youtu.be/2zQzQcX64vw). The main purpose of *TriCal* is to accurately position the device's TCP at the center of a sphere.

1) The measuring device

The *TriCal*'s measuring device is mounted on the robot via a tool changer. The mass of the *TriCal*'s measuring device is 1.7 kg (including all parts attached to the robot flange) with a position of center of gravity that meets ABB's load specifications.

The *TriCal* includes three Mitutoyo ID-C112XB indicators, which each have a resolution of 0.001 mm. These indicators are fixed, orthonormal to each other to a custom co-

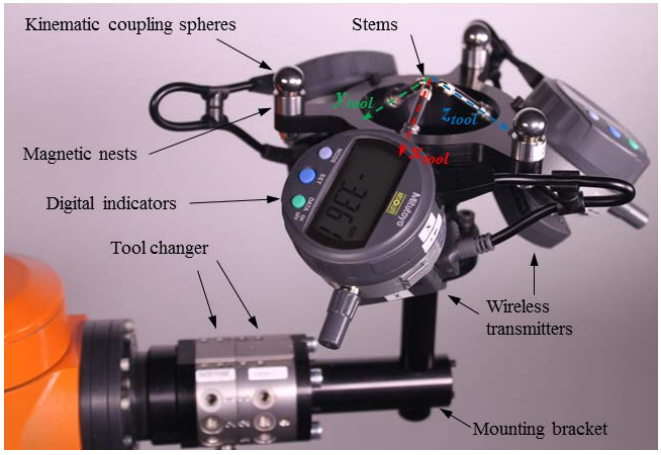

Figure 3. Components of the *TriCal*'s measuring device.

nical fixture (Fig. 3). A Mitutoyo U-WAVE-T wireless transmitter, attached on the back of each indicator, sends collected data to a Mitutoyo U-WAVE-R receiver, which is connected to a PC via a USB cable.

On the *TriCal*'s conical fixture, three 0.5-inch precision balls are temporarily attached to the magnetic nests, for the purpose of zeroing the device. These balls are called kinematic coupling spheres, and they are used to constrain the three dial indicators on the center sphere of the calibrator, as shown in Fig. 4. This process will be discussed further in Section IV.

2) The calibrator

The calibrator, as shown in Fig. 4, consists of a star-shaped bracket that holds three vee-grooves, a magnetic nest and a 0.5-inch precision ball (center sphere). It is used to set the device's TCP at the same position w.r.t. the conical fixture.

On the calibrator itself, the center sphere can be replaced with a standard spherically mounted retroreflector (SMR), to gather measurements with a laser tracker for validation. The calibrator's purpose is to accurately constrain the three digimatic indicators on the center sphere. Once the calibrator has been coupled with the measuring device, each indicator is manually set at zero. Thus, due to the calibrator, the TCP is always at the same position w.r.t. the main body (*i.e.*, the conical fixture) of the *TriCal*.

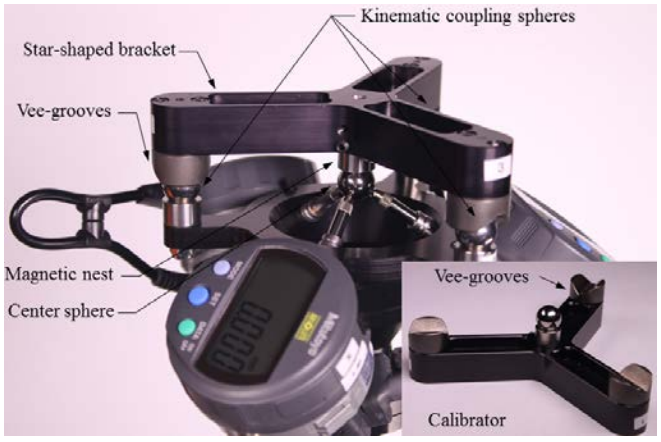

Figure 4. The *TriCal*'s measuring device and its calibrator.

IV. The Automated Measurement Process

This section will present the communication setup, describe the steps that must be performed before the *TriCal* can be used for calibration purposes, and explain the measurement automated procedure.

A. TriCal communication setup

To collect measurements without human intervention (*i.e.*, without an operator needing to push the send button on the transmitter), the U-Wave-Ts that are mounted on each digital indicator are set to "event driven" mode. In this mode, the data is transmitted automatically to the U-Wave-R every time the measurements on the digital indicators change. To access the data stored in the U-Wave-R, the user sends ASCII commands via MATLAB scripts using RS232 serial communication protocol. The information gathered in MATLAB is then sent to the robot controller via Ethernet communication (Fig. 5).

B. Preliminary steps

Three steps must be performed before the *TriCal* can be used for measurements. The first is zeroing the device: the manual initialization of the measuring device with the calibrator. The vee-grooves of the calibrator are positioned on the kinematic coupling spheres of the measuring device. Then, the set button is pressed on each indicator so that they are all zeroed. The calibrator and the three spheres can now be removed from the measuring device.

The second step is to locate the TCP (*i.e.*, the center of the calibrator's sphere) w.r.t. {6}, as accurately as possible. The measuring device is positioned so that all three stems of the digimatic indicators are in contact with a static target sphere (*i.e.*, the sphere to be measured). Then, by small iterative movements, the robot moves until all indicators read zero. This step is easy to do because the indicators are orthonormal, so the robot is moved according to the exact value displayed on each indicator. Once zero is reached, it means that the measuring device is constrained in the same way that it was when using the calibrator. The configuration can then be stored in the robot controller. This process is repeated three times, for a total of four random orientations, which are used to define the TCP w.r.t. {6}.

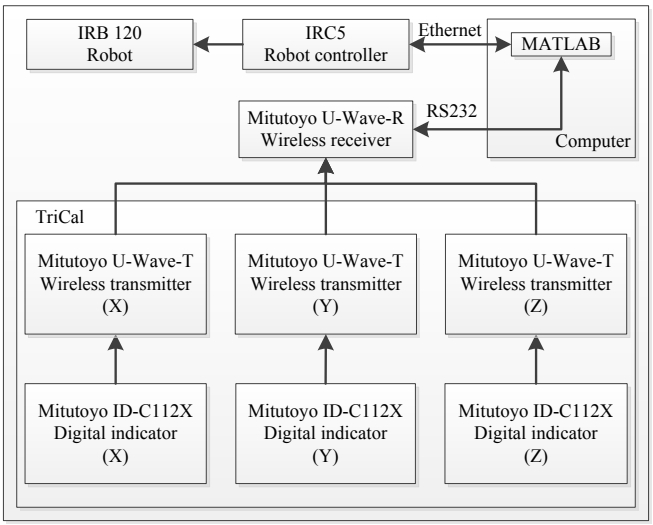

Figure 5. *TriCal* data flow.

The final step is to measure the position of each sphere on the triangular platform, so that $\{W\}$ can be defined. The three spheres are measured as in the previous step, but in only one orientation. Reference frame $\{W\}$ is then defined according to the steps in Section II.

C. The automated measurement procedure

For the *TriCal* to make a measurement, it must be constrained on a sphere. A minimum of three precision balls are required to define a reference frame, and to do an absolute calibration w.r.t. to this frame. In addition, the precise distances between the centers of these balls must be known. The automated measurement procedure is as follows:

(a) Move the robot until the *TriCal*'s three indicators touch the ball, at the desired joints configuration, $\mathbf{q}_d$.
(b) Send data request from MATLAB to the U-Wave-R.
(c) Receive measurements of all indicators, namely r_x, r_y and r_z, from U-Wave-R in MATLAB.
(d) Send r_x, r_y, and r_z from MATLAB to the robot controller.
(e) Displace the robot's TCP by the vector $\mathbf{r} = [r_x, r_y, r_z]$ w.r.t. $\{tool\}$.
(f) Repeat steps (b) to (e) until $\|\mathbf{r}\| < \varepsilon$, where ε is the maximum distance error allowed.
(g) In MATLAB, save the actual joints configuration, $\mathbf{q}_a$, that is given by the robot.
(h) Repeat steps (a) to (g) until all desired configurations have been measured.

The maximum distance error, ε, can be of any value. Ideally, its value would be zero, since this is the most precise measurement. However, if the value is below the robot's position repeatability, the measurement process takes a longer time to complete.

The collected measurements are the positions of the balls' centers w.r.t. $\{W\}$. Therefore, there are a total of three positions. Let $\mathbf{p}_{tool}^{W}$ be the position vector of $\{tool\}$ w.r.t. to $\{W\}$ that can be measured, and let d_{ij} be the distance measured between the centers of any two balls, i and j. The three position vectors that can be measured, which respectively represent the positions of balls 1, 2, and 3, are

$$\mathbf{p}_{tool}^{W} = [0,0,0] \ , \tag{6}$$

$$\mathbf{p}_{tool}^{W} = [d_{12},0,0] \ , \tag{7}$$

and

$$\mathbf{p}_{tool}^{W} = [x,y,0] \tag{8}$$

where

$$x = \frac{{d_{12}}^2 + {d_{13}}^2 - {d_{23}}^2}{2d_{12}} \ , \tag{9}$$

and

$$y = \sqrt{{d_{13}}^2 - x^2} \ . \tag{10}$$

V. Simulation

The simulation's purpose is to generate collision-free configurations, and to validate that the data from the *TriCal* enables accurate identification of the robot's parameters.

A. Generation of collision-free configurations

In order to simulate the real experiment, a set of n random robot configurations are generated at each sphere position with rotational constraints. A custom algorithm generates these configurations, according to the steps shown in Fig. 6.

When generating a new configuration, the algorithm evaluates what we refer to as "static collisions" and "dynamic collisions." Static collisions are collisions detected directly at a target configuration. Dynamic collisions are collisions detected while the robot is moving to the target configuration. In order to detect the static and dynamic collisions, we must simulate the complete measuring process and all its associated movements. For this purpose, the objects inside the workspace of the robot were modeled inside a virtual environment that features a collision detection module (RoboDK).

B. Assessment of the impact of measurement noise on the identification process

In order to validate the identification process, simulated errors were added to each parameter in realistic error ranges. Normally distributed errors of ±1 mm and ±1° were added for the distance and angular parameters, respectively. Normally distributed errors, ranging from -10^{-1} to -10^{-3} °/Nm, were added for the compliance parameters.

Towards the goal of better approximating the measurement noise, the following noise model is considered: the resolution of the digimatic indicators (±0.001 mm), the measurement procedure itself (±0.010 mm), the resolution of the telescoping ballbar (±0.0001 mm), and the tolerance of the precision balls' diameter (±0.0025 mm). The volumetric position accuracy was estimated to be around ± 0.020 mm. To account for these errors, an amplified normally distributed noise, of mean 0 mm and standard deviation 0.025 mm, was added to each measurement.

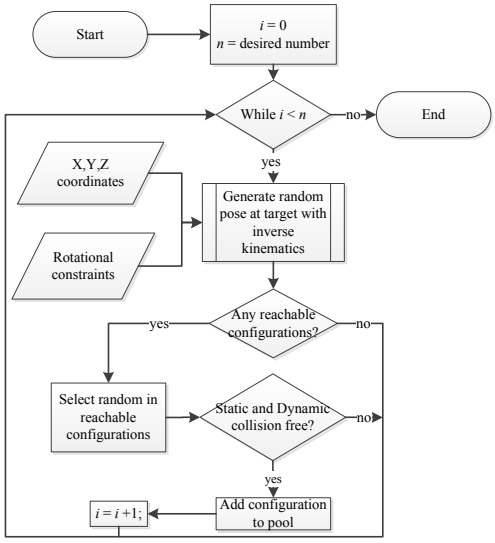

Figure 6. Algorithm for generating random robot configurations, free of static and dynamic collisions.

For the identification process, 45 configurations are selected randomly (15 for each sphere). These configurations simulate the measurements collected by the *TriCal* on the three balls. All measurements are taken w.r.t. to $\{W\}$.

To simulate the joint values measured on the robot, $\mathbf{q}_a$, when constrained at the requested calibration configuration, the inverse kinematics with the simulated parameters of the robot were computed. This computation was done both with and without the measurement noise. The linear least squares method [22] was used to identify the parameter values. To identify the compliance constants, the Newton-Euler algorithm, as presented in [21], was used to calculate the theoretical torques for each configuration. The masses and the positions of the centers of gravity for each link were provided by ABB. Table V presents the identification results from the simulation. Note that the parameters that were not selected for identification are not shown.

Naturally, parameters are to be accurately identified when no measurement noise is simulated. However, when noise is simulated, the parameters will be identified with errors. To validate the impact of the noise on the calibration, the identified parameters are used in two different simulations.

In the first simulation, we evaluate the influence of the noise on the calibration inside the target workspace. To do so, 100 random configurations are generated inside a sphere of 400 mm in diameter (Fig. 7), to simulate how they would be measured by a laser tracker.

TABLE V. SIMULATION – IDENTIFICATION OF PARAMETER VALUES

Parameters	Nominal	Simulated	Identified w/o noise	Identified w/ noise
x_0 (mm)	153.507	153.494	153.494	153.497
y_0 (mm)	−256.442	−256.362	−256.362	−256.336
z_0 (mm)	−228.116	−228.146	−228.146	−228.156
α_0 (°)	90.487	90.452	90.452	90.452
β_0 (°)	−1.054	−1.057	−1.057	−1.063
φ_0 (°)	−0.165	−0.068	−0.068	−0.068
x_{tool} (mm)	149.679	150.665	150.665	150.663
y_{tool} (mm)	1.859	0.993	0.993	0.989
z_{tool} (mm)	120.806	121.760	121.760	121.767
α_1(°)	−90.000	−90.049	−90.049	−90.048
α_2(°)	0.000	-0.076	−0.076	−0.074
α_3(°)	−90.000	−90.036	−90.036	−90.036
α_4(°)	90.000	90.024	90.024	90.024
α_5(°)	−90.000	−90.056	−90.056	−90.058
a_1 (mm)	0.000	0.064	0.064	0.065
a_2 (mm)	270.000	269.869	269.869	269.868
a_3 (mm)	70.000	70.125	70.125	70.139
a_4 (mm)	0.000	0.059	0.059	0.059
a_5 (mm)	0.000	−0.145	−0.145	-0.144
d_3 (mm)	0.000	0.136	0.136	0.131
d_4 (mm)	302.000	302.031	302.031	302.047
d_5 (mm)	0.000	−0.105	−0.105	−0.102
θ_2 (°)	−90.000	−90.000	−90.000	−90.003
θ_3 (°)	0.000	-0.006	−0.006	0.001
θ_4 (°)	0.000	0.018	0.018	0.018
θ_5 (°)	0.000	0.035	0.035	0.035
c_2 (°/Nm) * 10^{-3}	0.000	−2.634	−2.634	−2.787
c_3 (°/Nm) * 10^{-3}	0.000	−9.911	−9.911	−9.761
c_4 (°/Nm) * 10^{-3}	0.000	−8.817	−8.818	−9.097
c_5 (°/Nm) * 10^{-3}	0.000	−21.451	−21.451	−22.015
c_6 (°/Nm) * 10^{-3}	0.000	−79.040	−79.039	−81.077

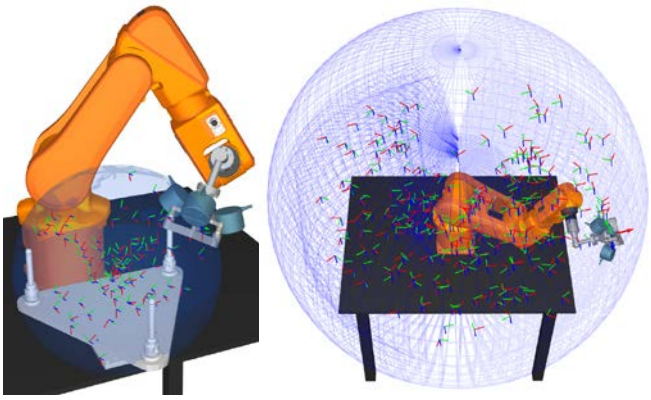

Figure 7. Random tool poses generated for measurements within the target workspace (left) and the whole robot workspace (right).

The configurations are generated using the same algorithm as the one presented in Fig. 6, but the input of the algorithm differs in two ways. First, the generated x, y, z coordinates are constrained inside the target workspace sphere, rather than at the three precisely-defined locations of the spheres. Second, because in the real experiment the configurations are measured with a laser tracker, the rotational constraints are changed so the *TriCal* constantly points toward the laser tracker.

In the second scenario, 500 configurations are generated inside the whole robot workspace (Fig. 7), by using the same algorithm to simulate how they would be measured with the laser tracker. The x, y and z coordinates are generated in the whole workspace of the robot, and the rotational constraints are fixed, so the *TriCal* constantly points toward the laser tracker in each configuration.

The simulated maximum position errors before calibration are 3.261 mm in the whole robot workspace and 2.515 mm in the target workspace. After calibration, the simulated maximum positions errors are reduced to 0.112 mm in the whole robot workspace and 0.026 mm in the target workspace. Clearly, the measuring noise of the *TriCal* affects the performance of the calibration.

In simulation, the position errors after calibration are very small compared to the experimental results because the theoretical model of the robot is considered to be the same as the real model. Thus, the simulated position errors after calibration do not include the impact of unmodeled parameters and leaves out other sources of errors, such as backlash in the gears, temperature, and the measurement uncertainty of the laser tracker.

VI. EXPERIMENTAL RESULTS

The actual experiment was divided into two main steps, which this section will describe in detail. First, we used the *TriCal* to measure the robot joint values needed for the identification process. After identifying the parameters of the robot, we then validated the performance of the calibration by using a laser tracker to measure positions inside the target workspace and in the whole workspace.

A. *Identification of the parameters*

The setup shown in Fig. 2 was used to obtain the measurements for the identification process. The 0.5-inch precision balls on the triangular platform have a diameter tolerance of ±0.0025 mm. The distances d_{ij} between the centers of each pair of balls were measured with a Renishaw telescopic ballbar, which has an uncertainty of ±0.001 mm. The room temperature was controlled to 22±0.3°C. A pool of 300 configurations was generated using the algorithm from Section V. Of these, 45 configurations were selected randomly for identification. The measurements for identification were obtained by probing the three precision balls on the triangular platform, according to the measuring procedure in Section IV. The maximum error allowed in the measuring procedure, ε, was set at 0.010 mm. After collecting the necessary measurements, the robot's parameters were identified using the linear least squares method. Table VI gives the parameter errors. We note that the compliance value of axis 6 is significantly higher than the other axes. This is explained by the fact that the torque applied on axis 6 is significantly lower than the other axes.

TABLE VI. EXPERIMENTAL IDENTIFICATION OF PARAMETER VALUES

Parameters	Nominal	Identified
x_0 (mm)	153.507	152.452
y_0 (mm)	−256.442	−254.866
z_0 (mm)	−228.116	−228.131
α_0 (°)	90.487	90.448
β_0 (°)	−1.054	−1.275
φ_0 (°)	−0.165	−0.155
x_{tool} (mm)	149.679	149.486
y_{tool} (mm)	1.859	1.679
z_{tool} (mm)	120.806	120.622
α_1 (°)	−90.000	−90.036
α_2 (°)	0.000	−0.035
α_3 (°)	−90.000	−89.957
α_4 (°)	90.000	89.997
α_5 (°)	−90.000	−90.002
a_1 (mm)	0.000	0.303
a_2 (mm)	270.000	270.066
a_3 (mm)	70.000	70.175
a_4 (mm)	0.000	−0.052
a_5 (mm)	0.000	0.008
d_3 (mm)	0.000	0.019
d_4 (mm)	302.000	302.075
d_5 (mm)	0.000	0.043
θ_2 (°)	−90.000	−90.067
θ_3 (°)	0.000	0.190
θ_4 (°)	0.000	−0.011
θ_5 (°)	0.000	0.068
c_2 (°/Nm) *10^{-3}	0.000	−4.289
c_3 (°/Nm) *10^{-3}	0.000	−3.099
c_4 (°/Nm) *10^{-3}	0.000	−14.834
c_5 (°/Nm) *10^{-3}	0.000	−17.986
c_6 (°/Nm) *10^{-3}	0.000	−91.752

B. *Validation*

The experimental validation used the same setup as that shown in Fig. 2, except that the configurations were measured with a FARO ION laser tracker, and not by constraining the indicators of the *TriCal*. The laser tracker has a measurement uncertainty of 0.049 mm, and it was placed approximately 3 m in front of the robot. The three 0.5-inch precision balls were replaced by three SMRs in order to measure $\{W\}$ with the laser tracker. After the three SMRs were measured, the triangular platform was removed from the robot workspace. The calibrator was attached to the measuring device with a rubber band, and the center sphere was replaced by a 0.5-inch SMR. The validation used the 500 configurations generated previously in the simulation.

The *TriCal*'s calibration performance is clearly better inside the 400 mm sphere than within the whole workspace, as shown in Table VII. With further analysis, we found that the poor performance of the calibration in the whole workspace correlates with the angular positions of joint 2. Figure 8 shows that the position errors grow exponentially when $\theta_2 < -32°$, the smallest value used in the identification phase for joint 2. Thus, by limiting the minimum angle for joint 2 to $\theta_2 > -32°$ on the 500 configurations, the results are significantly better, as shown in Table VIII, while this still covering a very large portion of the whole workspace.

The final step of the validation was to plot the position errors after calibration in this new constrained workspace, as a function of the distance of the TCP from the center of the target workspace. From the resulting plot, shown in Fig. 9, we observe that the greater the distance between the TCP and the target workspace center, the greater the position errors. This confirms our initial assumption that the device presents a better performance for local calibration.

TABLE VII. POSITION ERRORS BEFORE AND AFTER CALIBRATION

	Position Errors in Target Workspace		Position Errors in Whole Workspace	
	Before cal.	***After cal.***	***Before cal.***	***After cal.***
Mean (mm)	1.114	0.272	1.688	0.804
Max (mm)	1.726	0.491	4.567	2.839
Std (mm)	0.336	0.108	0.793	0.703
Median (mm)	1.212	0.290	1.536	0.488

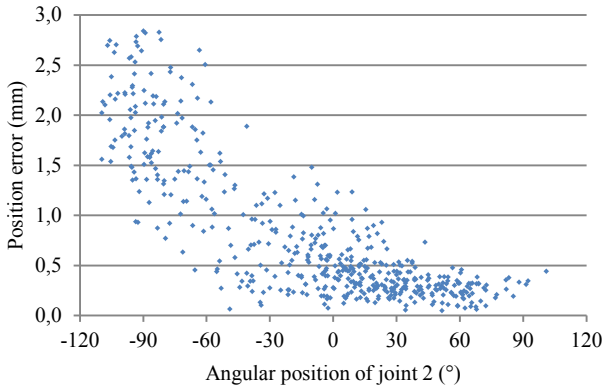

Figure 8. Position errors w.r.t. the angular position of joint 2 on the 500 configurations used for validation in the whole workspace.

TABLE VIII. POSITION ERRORS AFTER CALIBRATION – WHOLE WORKSPACE VS CONSTRAINED WORKSPACE

Position errors	Whole workspace (no joint limits)	Constrained workspace ($\theta_2 > -32°$)
Mean (mm)	0.804	0.426
Max (mm)	2.839	1.480
Std (mm)	0.703	0.260
Median (mm)	0.488	0.355

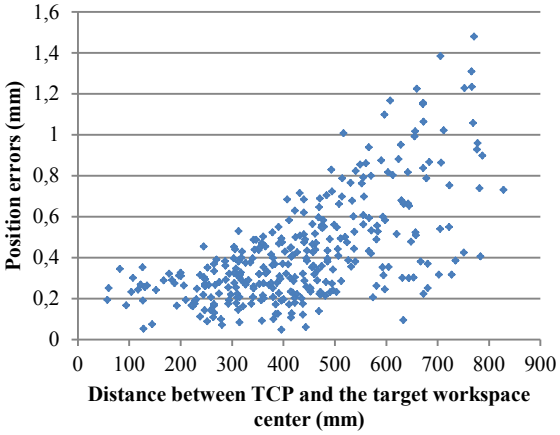

Figure 9. Position errors after calibration in the constrained workspace.

VII. CONCLUSION

In this paper, we presented a novel measuring device, and an automated measurement method, for the calibration of six-axis industrial robots inside a target workspace. The measuring device has the advantage of being low-cost, accurate, and portable. Furthermore, the measuring method is fully automated and quickly performed.

As expected, the calibration results are better inside a target workspace than in the whole workspace, with a maximum position error of 0.491 mm. This is because the calibration configurations were only intended to be inside the target workspace, since the goal of this work is to improve the accuracy inside that workspace.

It is interesting to note that another low-cost pose measuring device, which we introduced in [12] and which is based on a single Renishaw ballbar, was also used for calibrating another small robot, the FANUC LR Mate 200iC [22]. The position accuracy after calibration was very similar to what we were able to achieve with the *TriCal*. However, our Renishaw ballbar-based pose-measuring device cost about US$20,000, whereas the *TriCal* is less than US$5,000, and the *TriCal* allows the calibration process to be fully automated. The price of the *TriCal* includes all its parts, except the ballbar, which can be replaced with any other external measurement device. Of course, both devices are low-cost compared to a laser tracker, which may cost more than US$100,000.

Future work should further analyze the size, shape and position of the calibration platform. Also, the optimal positions and number of precision balls, as well as the optimal set of configurations for identification could be assessed based on observability [8]. Finally, it could prove fruitful to study the use of the *TriCal* for repeatability analysis.

REFERENCES

[1] B. Mooring, M. Driels, and Z. Roth, *Fundamentals of Manipulator Calibration*: John Wiley and Sons, Inc., 1991.

[2] A. Y. Elatta, G. Li Pei, Z. Fan Liang, D. Yu, and F. Luo, "An overview of robot calibration," *Information Technology Journal,* vol. 3, pp. 74-8, 01/ 2004.

[3] J. Denavit and R. S. Hartenberg, "A kinematic notation for lower-pair mechanisms based on matrices," *Trans. of the ASME. Journal of Applied Mechanics,* vol. 22, pp. 215-221, // 1955.

[4] S. A. Hayati, "Robot arm geometric link parameter estimation," in *Decision and Control, 1983. The 22nd IEEE Conference on*, 1983, pp. 1477-1483.

[5] K. Okamura and F. C. Park, "Kinematic calibration using the product of exponentials formula," *Robotica,* vol. 14, pp. 415-21, 07/ 1996.

[6] H. Zhuang, Z. S. Roth, and F. Hamano, "A complete and parametrically continuous kinematic model for robot manipulators," *Robotics and Automation, IEEE Transactions on,* vol. 8, pp. 451-463, 1992.

[7] H. W. Stone, A. C. Sanderson, and C. P. Neuman, "Arm signature identification," in *Robotics and Automation. Proceedings. 1986 IEEE International Conference on*, 1986, pp. 41-48.

[8] J.-H. Borm and C.-H. Menq, "Determination of optimal measurement configurations for robot calibration based on observability measure," *International Journal of Robotics Research,* vol. 10, pp. 51-63, 1991.

[9] A. Joubair, M. Slamani, and I. A. Bonev, "Kinematic calibration of a 3-DOF planar parallel robot," *Industrial Robot: An International Journal,* vol. 39, pp. 392-400, 2012.

[10] A. Joubair and I. A. Bonev, "Kinematic calibration of a six-axis serial robot using distance and sphere constraints," *The International Journal of Advanced Manufacturing Technology,* vol. 77, pp. 515-523, 2015.

[11] A. Joubair and I. A. Bonev, "Non-kinematic calibration of a six-axis serial robot using planar constraints," *Precision Engineering,* vol. 40, pp. 325-333, 2015.

[12] A. Nubiola, M. Slamani, and I. A. Bonev, "A new method for measuring a large set of poses with a single telescoping ballbar," *Precision Engineering,* vol. 37, pp. 451-460, 2013.

[13] T. Huang, Z. Y. Hong, J. P. Mei, and D. G. Chetwynd, "Kinematic Calibration of the 3-DOF Module of a 5-DOF Reconfigurable Hybrid Robot using a Double-Ball-Bar System," in *Intelligent Robots and Systems, 2006 IEEE/RSJ International Conference on*, 2006, pp. 508-512.

[14] A. Nubiola, M. Slamani, A. Joubair, and I. A. Bonev, "Comparison of two calibration methods for a small industrial robot based on an optical CMM and a laser tracker," *Robotica,* vol. 32, pp. 447-466, 2014.

[15] M. Švaco, B. Šekoranja, F. Šuligoj, and B. Jerbić, "Calibration of an Industrial Robot Using a Stereo Vision System," *Procedia Engineering,* vol. 69, pp. 459-463, // 2014.

[16] G. Zak, B. Benhabib, R. G. Fenton, and I. Saban, "Application of the Weighted Least Squares Parameter Estimation Method to the Robot Calibration," *Journal of Mechanical Design,* vol. 116, pp. 890-893, 1994.

[17] K. English, M. J. D. Hayes, M. Leitner, and C. Sallinger. (2002). *Kinematic Calibration of Six-Axis Robots*.

[18] H. J. Warnecke, M. Week, B. Brodbeck, and G. Engel, "Assessment of Industrial Robots," *CIRP Annals - Manufacturing Technology,* vol. 29, pp. 391-396, // 1980.

[19] D. J. Bennett and J. M. Hollerbach, "Autonomous calibration of single-loop closed kinematic chains formed by manipulators with passive endpoint constraints," *Robotics and Automation, IEEE Transactions on,* vol. 7, pp. 597-606, 1991.

[20] M. A. Meggiolaro, G. Scriffignano, and S. Dubowsky, "Manipulator calibration using a single endpoint contact constraint," in *Proceedings of ASME Design Engineering Technical Conference, Baltimore, USA*, 2000.

[21] J. J. Craig, *Introduction to robotics: mechanics and control 3rd edition* vol. 3: Pearson Prentice Hall Upper Saddle River, 2005.

[22] A. Nubiola and I. A. Bonev, "Absolute robot calibration with a single telescoping ballbar," *Precision Engineering,* vol. 38, pp. 472-480, 7// 2014.